IAC-18-D4.IP.6.42722

TETHERED SLINGSHOT MANEUVER IN THE THREE-DIMENSIONAL SPACE

Alessandra F. S. Ferreira*
São Paulo StateUniversity – UNESP, Brazil, alessandra.ferraz@unesp.br

Rodolpho V. Moraes
São Paulo State University – UNESP, Brazil,
National Institute for Space Research - INPE, Brazil, rodolpho.vilhena@gmail.com

Antonio F. B. A. Prado
National Institute for Space Research - INPE, Brazil, antonio.prado@inpe.br

Othon C. Winter
São Paulo State University – UNESP, Brazil, othon.winter@unesp.br

* Corresponding Author

Abstract

The Tethered Slingshot maneuver (TSSM) is an alternative solution to maneuver a spacecraft in space, which is based in the use of cables. A space tether usually consists in two fixed objects at the end of a cable. In this work, it will be considered a cable anchored in a celestial body, which can be a planet, a moon or an asteroid and, at the other end, a spacecraft. The cable is considered to be thin, rigid, inextensible and with negligible mass. The purpose of the maneuver is to change the energy and/or inclination of the spacecraft using a rotation around a celestial body made by a tether attached to it. The energy gain obtained by the Tethered Slingshot Maneuver will be analyzed. The rotation made in the spacecraft makes significant modifications in the trajectory of the spacecraft when compared to maneuvers using only gravity, in particular when the bodies are small. The maneuver is analyzed in the three-dimensional space. The solutions were presented for two different asteroid systems and the results were made and analyzed for different variables of the system.

Keywords: Tethered Slingshot Maneuver, Tether, spacecraft, orbital maneuvers.

1. Introduction

Space Tethers has been studied recently in various applications. Starting with its configuration, it can have two spacecraft fixed at the ends of a cable or a celestial body (like planet, moon or asteroid) fixed at one end and the spacecraft fixed at the other [1-9].

Its function may be to generate energy to the spacecraft, to transfer or control the spacecraft in orbit, to make transportation and communication or to build space elevators [3,5-6,8,10]. Regarding transfers or control of a spacecraft in orbit, there are some works available in the literature, in particular about the Tethered Slingshot maneuver (TSSM) [11-18]. They show its use for spacecraft capture or escape, usually limiting the motion of the tether to the plane of the primary bodies (two-dimensional space) [16-18]. Others show the analysis of the equilibrium points of a tether [19-20]. Among them, there are studies considering irregular bodies, with the objective of applying techniques using tethers in double asteroid systems [20-21].

In TSSM, the spacecraft approaches the celestial body, connects to the tether, and then it rotates around the celestial body by a given angle. After that the spacecraft is released from the cable to complete the maneuver and assume a new trajectory. The rotation suffered by the spacecraft makes significant modifications in its trajectory, when compared to an equivalent pure gravity Swing-By maneuver with the same body. The main difference is that, in particular for bodies with low mass, the effect coming only from gravity is small, so the tether can give a significant increase in the energy gain for the spacecraft.

The cable is considered to be thin, rigid, inextensible and with negligible mass. It can measure from a few

meters to thousands of kilometers. The mechanism of the structure that will receive the spacecraft and its installation in the celestial body will not be discussed in this work, which is devoted in studying the astrodynamics aspects of the maneuver. The idea is to show a potential that exist in nature and that, sooner or later, will be used to send spacecrafts to points distant from the Earth.

The rotation from the tether and the trajectory of the spacecraft occur in the three-dimensional space, so covering more real cases and more possible applications.

The objective is to analyze the energy gain and the variation in the inclination of the spacecraft and the resulting types of orbits, with respect to the main body of the system, which is obtained from the maneuver.

For the numerical simulations, the systems Sun-Vesta and Sun-Apophis are used.

2. Literature review

The Tethered Slingshot Maneuver has similarities with the pure "Gravity Assisted Maneuver" [22-23]. Its configuration makes the spacecraft to rotate around the celestial body for a given angle, so changing its trajectory. For the "Gravity Assisted Maneuver" or “Swing-By Maneuver”, the spacecraft passes close to the celestial body and uses the gravity of this body to modify the trajectory. There are studies available that combine gravity with the application of an impulse at the time of the close encounter to optimize the gain or loss of energy of the spacecraft in the plane [24-28].

The main advantage of the maneuver based on tethers is that the gains of energy are much larger when compared to the equivalent gravity maneuver. This applies mainly when a small body is considered, like an asteroid or a small moon of a planet. The gravitational field of these small bodies are very weak, giving small angles of rotation for the gravity maneuver, which results in small variations of energy. Therefore, the use of tethers can give a larger angle of rotation and, consequently, greater variation in the energy.

The application of the maneuver in the three-dimensional case may also be associated with a three-dimensional Swing-By maneuver [29], in which the spacecraft approaches the body at an angle inclined to the plane of the primaries.

3. Statement of the problem

The problem uses the model given by the Circular Restricted Three-Body Problem (CRTBP) [30], being M_1 the most massive body, M_2 the secondary body, where the tether will be fixed; and M_3, the spacecraft with negligible mass and that will connect to the other end of the tether to make the rotation.

The particular case of maneuvers developed in a plane that intercepts the reference plane in the y-axis is considered. The location of this plane can be defined by the angle β. Figure 1 describes the maneuver in the reference system x', y', z', which is centered on M_2. The spacecraft approaches M_2, coming from an orbit around M_1, connects to the tether and the rotation is done in this plane defined by the angle β. The rotation is denoted by 2δ, and it is measured from the point of the connection of the spacecraft with the device to the point where it leaves the tether, which is again an orbit around M_1. The projection of this maneuver in the $x' - y'$ plane is presented. α is the angle that defines the location of the middle point of the rotation. In this point (α) the velocity is given by V. l is the size of the cable.

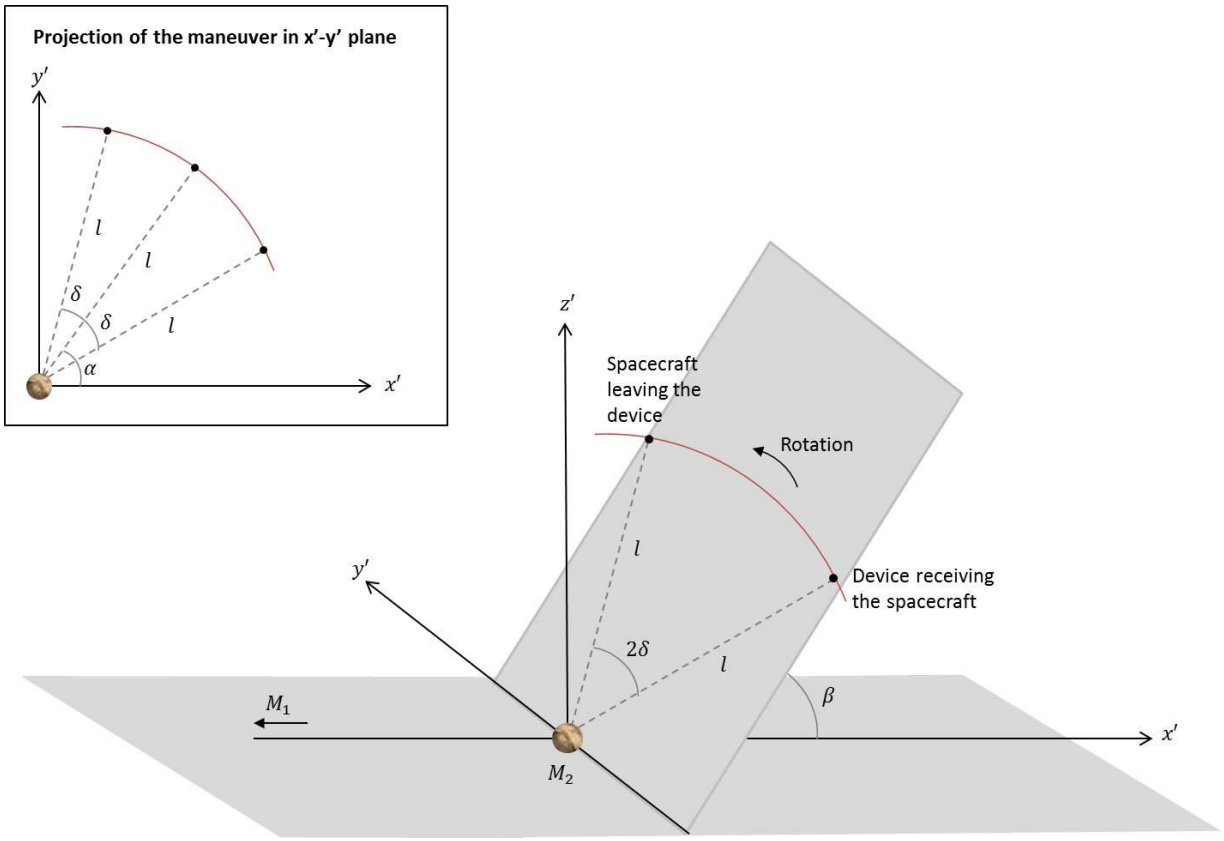

Fig. 1. Geometry of the TSSM.

The position and velocity of the spacecraft at the instants that the device receives and releases the spacecraft, measured from the center of mass of the system, are now presented. After these initial conditions are defined, they are numerically integrated for a given time to obtain the results.

$$\begin{aligned} x &= (1-\mu) + l\cos(\alpha \pm \delta)\cos\beta \\ y &= l\,sin(\alpha \pm \delta)\cos\beta \\ z &= l\,sin\,\beta \end{aligned} \tag{1}$$

$$\begin{aligned} V_x &= -V\,sin(\alpha \pm \delta) + l\,sin(\alpha \pm \delta)\cos\beta \\ V_y &= Vcos(\alpha \pm \delta) - l\cos(\alpha \pm \delta)\cos\beta \\ V_z &= 0 \end{aligned} \tag{2}$$

Where applicable, $\pm$ represents "$-$" when the tether receives the spacecraft and "$+$" is used when it disconnects the spacecraft to allow it to follow its trajectory.

The energy and angular momentum of the spacecraft relative to the primary body at the instant before (E_-, C_-) and after (E_+, C_+) the maneuver are obtained. From this, it is obtained the variation of energy $\Delta E = E_+ - E_-$, which quantifies the gain or loss of energy due to the TSSM. The variation of the inclination $\Delta I = i_+ - i_-$, being $i = cos^{-1}\left(\frac{C_z}{|C|}\right)$ and C_z the component z of angular momentum.

About the characteristics of the orbits before and after the rotation, the following possibilities exist:

- Direct ellipse: $E < 0$ and $C > 0$;
- Retrograde ellipse: $E < 0$ and $C < 0$;
- Direct hyperbole: $E > 0$ and $C > 0$;
- Retrograde hyperbole: $E > 0$ and $C < 0$;

From this information, Table 1 classifies the types of possible orbits resulting from a TSSM.

Table 1. Classification of the orbits.

After: / Before:	Direct ellipse	Retrograde ellipse	Direct hyperbole	Retrograde hyperbole
Direct ellipse	A	E	I	M
Retrograde ellipse	B	F	J	N
Direct hyperbole	C	G	K	O
Retrograde hyperbole	D	H	L	P

Orbits of type 'Y' and 'Z' may also occur. 'Y' means that the spacecraft collided with the surface of the secondary body during the integration time. 'Z' means that the spacecraft was captured by the gravity of the secondary body and stayed around it during the total integration time.

4. Results

The energy and inclination variations and the types of orbits resulting from the maneuver will be studied. The analysis of the results will be made for the different controllable variables of the system. The size of the cable l is fixed at 100 km for all cases. According to Prado [16-17] the variation of energy is independent of the cable size. For the initial conditions adopted, showed in Fig. 1, the energy variation is independent of β. Its main influence is in the change in the inclination of the orbit.

To verify the minimum velocity that a spacecraft has when arriving at M_2, a "Patched-Conic" approximation is used in a Hohmann type maneuver, considering the transfer orbit tangent to the orbit of the asteroid.

The asteroids systems Vesta and Apophis are used for the numerical simulations. They are both moving around the Sun, but with different characteristics of mass, size and distance.

4.1 Sun-Vesta system

Vesta [31] is in the asteroid belt, a region between the orbits of Mars and Jupiter, about 2.36 AU from the Sun. Its radius is approximately 262.7 km, its mass 2.67×10^{20} kg and its orbital velocity 19.34 km/s, assuming a circular orbit.

Figure 2 shows the energy variation as function of α in the x-axis and δ in y-axis, for an approaching velocity of $V = 8.8$ km/s. Note that the main influence in the energy variation comes from α. This variable defines if the variation is positive or negative. If positive, the spacecraft gained energy after the rotation and, if negative, it loses energy. It is like the gravity maneuver. If the spacecraft passes in front of the body, $0° < \alpha < 180°$, it is decelerated by to gravity of M_2 and it loses energy. If $180° < \alpha < 360°$, the spacecraft passes behind M_2 and then it is accelerated by the gravity of M_2, so gaining energy [22]. Still based on Broucke's definitions [22], observe that the energy variation is null for $\alpha = 0°$ and $\alpha = 180°$, minimum for $\alpha = 90°$ and maximum for $\alpha = 270°$. Regarding δ, the variation ranges from 0° to 90°, being the rotation equal to 2δ, so the maximum would be 180°. In this interval there is no risk of the cable to wrap around the surface of the body during the rotation. The main effect of δ in the maneuver is on the magnitude of the energy variation. The larger the rotation the greater the magnitude.

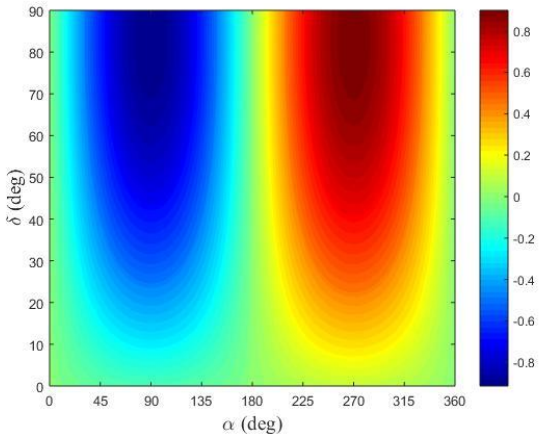

Fig. 2. Energy variation (in km²/s²) for $V = 8.8$ km/s.

Figure 3 analyzes the effect of the approach velocity and the rotation angle in ΔE, considering $\alpha = 270°$. Higher speeds combined with higher rotation angles result in maximum energy gains for this configuration. The maximum gain is approximately 4.0 km²/s².

If $\alpha = 90°$, the maximum energy variation in magnitude also occurs for the higher values of δ. But, in those cases, where ΔE is negative, the spacecraft loses energy after the rotation.

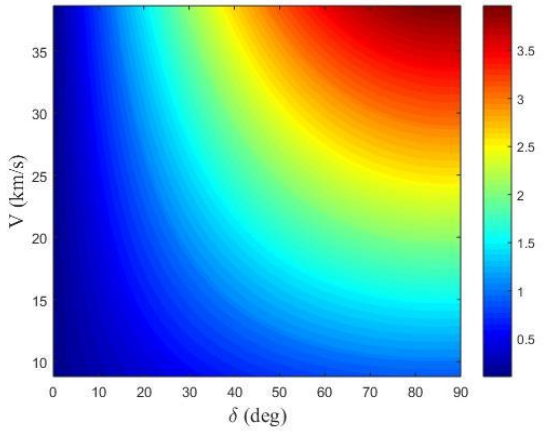

Fig. 3. Energy variation (in km²/s²) for $\alpha = 270°$.

Analyzing the energy variation due to α and the velocity V (Fig. 4), for $\delta = 90°$, it is seen that the region of gain or loss of energy after the rotation of the spacecraft is limited by $\alpha = 180°$ and that the greater the speed the greater the magnitude of the gain or loss of energy. The velocity ranges from 8.8 km/s to twice the orbital velocity of Vesta.

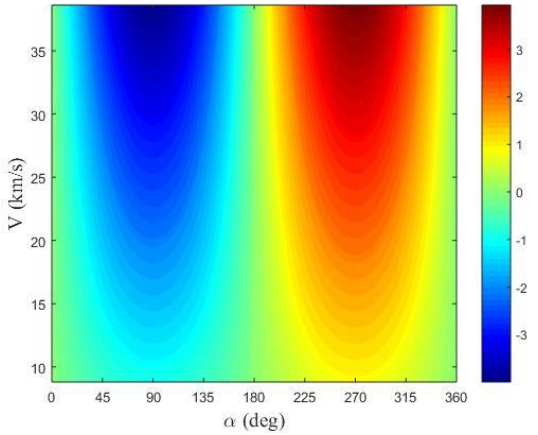

Fig. 4. Energy variation (in km²/s²) for $\delta = 90°$.

The analysis on the change in the inclination (ΔI) was also made and the main factor influencing in this variation is β, as expected.

Figure 5 shows the variation in the inclination for $\delta = 90°$ and $V = 8.8$ km/s. In ΔE positive region, the variation of inclination is negative. That is, when the spacecraft gains energy after the maneuver, the inclination decreases. The inclination of the orbit tends to zero for the cases with maximum energy. The maximum magnitude is approximately 4.9°.

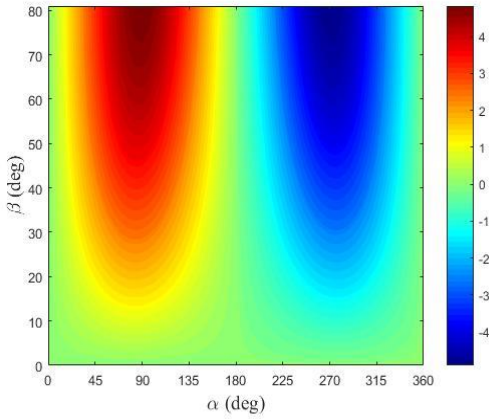

Fig. 5. Inclination variation (in degrees) for $\delta = 90°$ and $V = 8.8$ km/s.

Figure 6 shows the variation in the inclination of the orbit of the spacecraft. For all combinations of the conditions. The orbit before the maneuver was more inclined than the orbit obtained after the maneuver, because ΔI is always negative. The largest discrepancies in the magnitude of the inclination between the two orbits occur for the highest values of β and the angle of rotation. The absolute maximum value is approximately 4.97°.

This plot shows the similar effects in ΔI for the out-of-plane component (β) and rotation angle (δ), for the conditions studied.

For the case $\alpha = 90°$, the variation is positive and the magnitude similar to what was shown in Fig. 6.

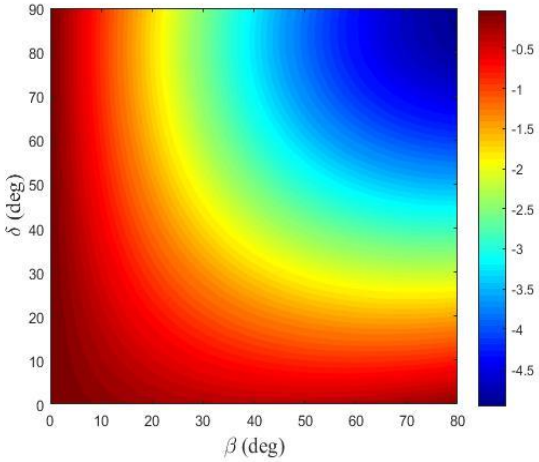

Fig. 6. Inclination variation (in degrees) for $\alpha = 270°$ and $V = 8.8$ km/s.

Figure 7 shows the variation of inclination as a function of β and V, for $\alpha = 270°$ and $\delta = 90°$.

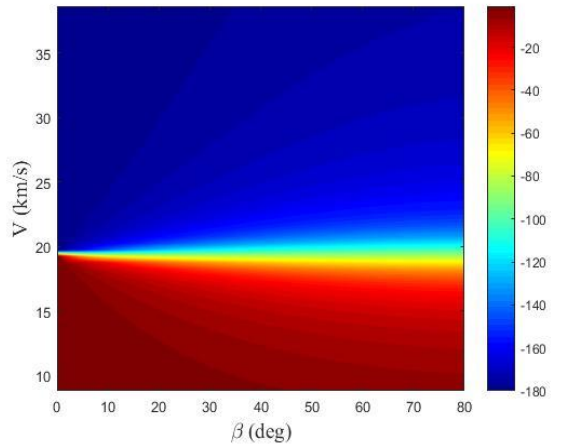

Fig. 7. Inclination variation (in degrees) for $\alpha = 270°$ and $\delta = 90°$.

The variation in inclination is always negative, reaching up to 180° for the highest speed values. We can deduce that, for the same conditions, the energy variation is always positive, the spacecraft gains energy after the maneuver but loses inclination. β gives smaller variations in inclination from one condition to another (see that the curves are smoothly inclined) and V makes a subdivision into $\Delta I: V < \sim 19$ km/s $\rightarrow \sim 0° < \Delta I < -40°$; V around 20 km/s $\rightarrow \sim -40° < \Delta I < -14$; $V > \sim 20$ km/s $\rightarrow \sim -140° < \Delta I < -180°$.

To finalize the analysis of the TSSM in Vesta, the variations in the types of orbits due to the maneuver, for α and V varying and $\delta = 90°$, are presented in Fig. 8. The plots are based on Table 1.

The plots are functions of α (in x-axis) and velocity of approach, in y-axis. The velocity of approach is varying from approximately 8.8 km/s to 38.68 km/s, which is equals to twice of the orbital velocity of Vesta.

The orbits ‘C’ and ‘G’ result in the capture of the spacecraft by the primary body. The spacecraft began the maneuver in a hyperbolic orbit and, after the maneuver is completed, the new orbit became elliptic direct for ‘C’ and retrograde for ‘G’. The orbits ‘I’ and ‘J’ characterize the escape of the spacecraft from the system, which means that, initially, the orbit was direct elliptical for 'I' and retrograde for ‘J’, ending in a hyperbole prograde after the maneuver. Both cases are highlighted in gray on the plot. Note that retrograde orbits always occur when the approach velocity is greater than the orbital velocity of the secondary body. The capture cases occurred for α lower than 180°, a region where the maneuver decelerates the spacecraft, decreasing its velocity and energy with respect to M_1. For α greater than 180°, escapes occurred.

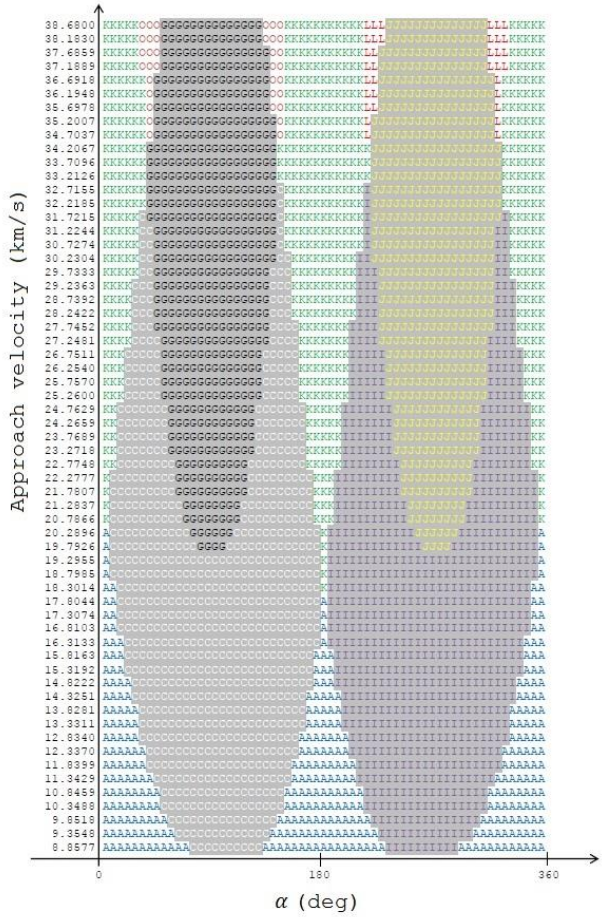

Fig. 8. Types of orbits for $\delta = 90°$ and $\beta = 45°$.

For the ‘K’, ‘L’ and ‘O’ classifications, the spacecraft comes from an open orbit and keeps it open. ‘L’ and 'O' are classification of orbits that change only the direction of motion. In ‘A’ the approach is in a direct elliptical orbit, which remains after the maneuver.

4.2 Sun-Apophis system

99942 Apophis [32] is a Near-Earth asteroid that belongs to group Aten (Earth crossing asteroids with semi-major axes smaller than 1 AU). Its semi-major axis is 0.9224 AU. Its radius is approximately 162.5 m, its mass 2.7×10^{10} kg and its orbital velocity 30.728 km/s, assuming a circular orbit for Apophis.

The energy variation as function of α in the x-axis and δ in the y-axis, for $V = 25.0$ km/s, is shown in Fig. 9.

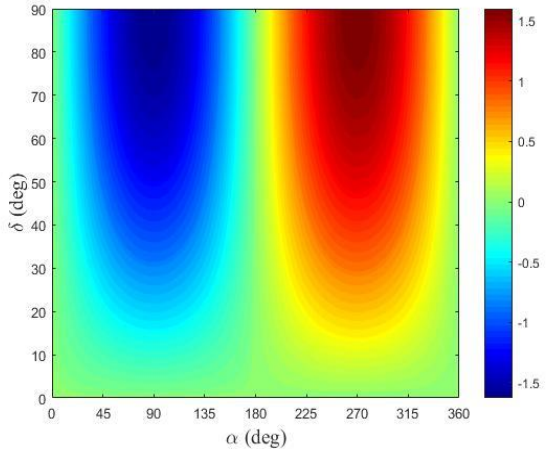

Fig. 9. Energy variation (in km²/s²) for $V = 25.0$ km/s.

The energy is higher in the second orbit than in the first one, before the maneuver, when the tether receives the spacecraft in α between 180° and 360°, as already explained. The behavior is similar to the one observed in Vesta, but the magnitude of ΔE for this system is larger, reaching up to approximately 1.6 km²/s².

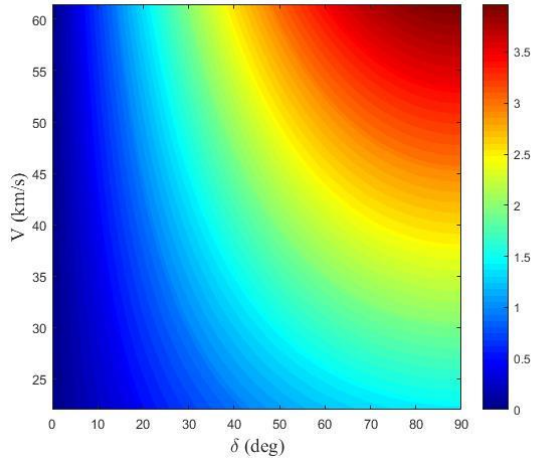

Fig. 10. Energy variation (in km²/s²) for $\alpha = 270°$.

Figure 10 shows the effect in ΔE of the rotation angle (δ) and the approach velocity (V). Note that the energy increases in the second orbit as δ and V increase. The maximum energy gain is approximately 4.0 km²/s².

Figure 11 shows the energy variation as a function of α and V, considering $\delta = 90°$.

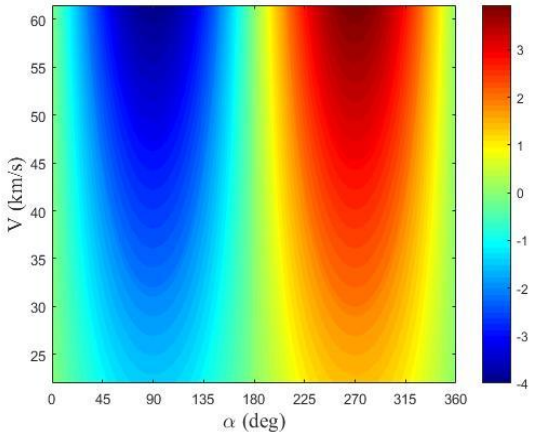

Fig. 11. Energy variation (in km²/s²) for $\delta = 90°$.

In Fig. 11, the velocity generates soft curves in parabolic forms for the energy variations, gradually changing the magnitude, since α is known to define the gain or loss of energy. The maximum magnitude is 4.0 km²/s².

The following is the variation of the inclination, whose main influence is the angle β. Figures 12, 13 and 14 show ΔI for $\alpha \times \beta$, $\beta \times \delta$ and $\beta \times V$, respectively.

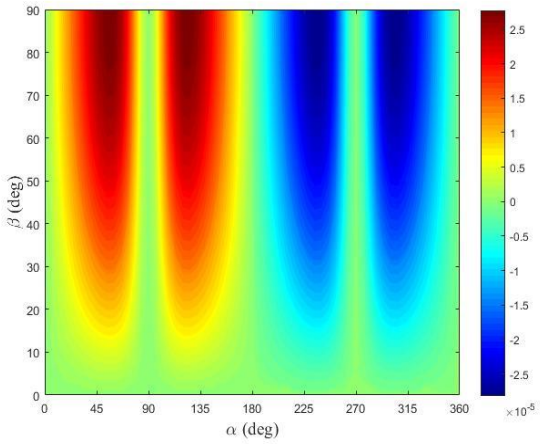

Fig. 12. Inclination variation (in degrees) for $V = 25.0$ km/s and $\delta = 90°$.

Figure 12 shows that the magnitude of the variation is of the order of 10^{-5} km²/s². It also shows that the change in the inclination was small. Observe that, for $\alpha = 90°$ and $\alpha = 270°$, the energy variation is zero, dividing the map into two sets of gains and losses of energy, with two points of maximum and minimum.

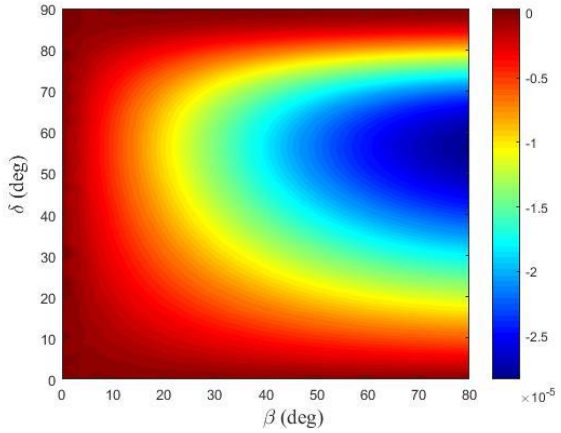

Fig. 13. Inclination variation (in degrees) for $\alpha = 270°$ and $V = 25.0$ km/s.

Figure 13 shows that the magnitude of the variation of the inclination is also of the order of 10^{-5} km²/s², decreasing after the maneuver ($\Delta I < 0$). Note that the out-of-plane component (β) has a significant effect on the inclination and that the largest magnitudes occur for median values of δ. In these cases the spacecraft is closer to the plane of rotation in the second orbit than in the first one, before the maneuver.

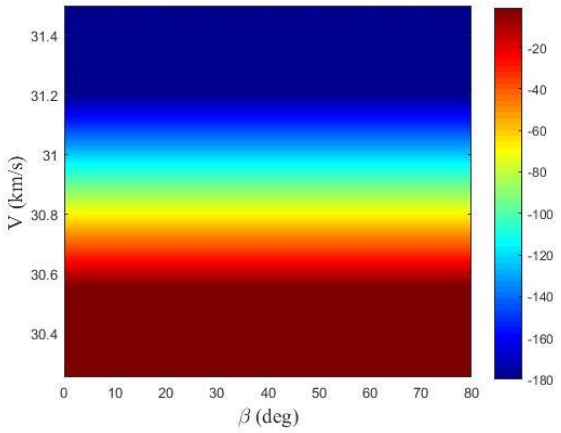

Fig. 14. Inclination variation (in degrees) for $\alpha = 270°$ and $\delta = 90°$.

In Fig. 14, the main influence is the velocity. The variation of the inclination is equal to $-180°$ for V approximately greater than 31.2 km/s and 0° for V less than 30.6 km/s.

The resulting types of orbit of the TSSM for the Sun-Apophis system were also verified.

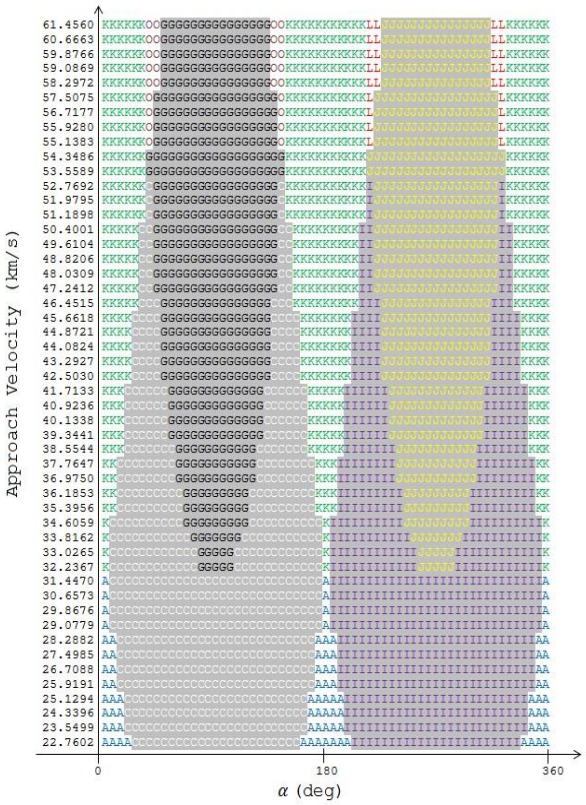

Fig. 15. Types of orbits for $\delta = 90°$ and $\beta = 45°$.

Note that the capture ('C' and 'G') and escape ('I' and 'J') orbits of the spacecraft by the primary body occur for $\alpha = 90°$ and $\alpha = 270°$, respectively, as expected. Being the retrograde orbits just above the orbital velocity of M_2. There are few cases of unchanged types of orbits 'K', 'L' and 'O'. In these classifications, the spacecraft comes from an open orbit and remain in an open orbit after the maneuver. Only 'L' and 'O' change the direction of motion of the spacecraft. In orbits type 'A' the spacecraft comes from a direct closed orbit and keeps it in that way.

5. Conclusions

The evolution of a "Tethered Slingshot Maneuver" (TSSM) in three-dimensional space, considering the particular case of maneuver developed in a plane that intercepts the reference plane in the y-axis was presented.

The solutions were exemplified for two different asteroid systems by maps of the variation of energy, inclination and classification of the types of orbits resulting from the maneuver with respect to the main body.

The analyze of the results were made for different controllable variables of the system, being α the angle that defines the gain or loss energy region. β is the main influence on inclination variation, but the

energy variation is independent of it. The change in inclination increases with the increase in the magnitude of β. The rotation angle 2δ is limited to 180°, to avoid the wrapping of the cable around the Moony. It increases the magnitude of the variation of the gain or loss of energy.

The spacecraft's largest energy gains occur in orbits near the orbital plane of the primaries. The lower the energy gain the greater the inclination of the orbit.

Regarding the types of orbits obtained from the TSSM, the highest occurrence for the initial conditions used were cases where the spacecraft is captured by the main body and escape out of the system. Captures occurred around $\alpha = 90°$, region of energy loss and escapes around $\alpha = 270°$, region of energy gains.

Acknowledgements

The authors wish to express their appreciation for the support provided by the National Council for Scientific and Technological Development (CNPq), the grants #300923/2017-1, 406841/2016-0, 301338/2016-7 and 312813/2013-9; Sao Paulo Research Foundation (FAPESP), the grants #2016/14665-2, 2016/24561-0 and 2016/23542-1.

References

[1] Artsutanov, Y. N. The Earth-to-Moon highway. Technnics for Youth, No. 4, 21, 35, 1979 (In Russian).

[2] Pearson, J. Lunar Anchored Satellite Test. Proceedings AIAA/AAS Astrodynamics Conference, AIAA 78-1427, August 1978.

[3] Pearson, J. Anchored Lunar Satellites for Cislunar Transportation and Communication. Journal of the Astronautical Sciences. Vol. XXVII, No. 1, pp. 39-62, 1979.

[4] Beletsky, V.V., Levin, E.M. Dynamics of lunar tether system. Cosmic Research, Vol. 20, No. 5, pp. 760-764, 1982.

[5] Pearson J., Levin E., Oldson J., Wykes H. The Lunar Space Elevator. IAC-04-IAA.3.8.3.07, 55th International Astronautical Congress, Vancouver, Canada, October 4-8 2004.

[6] Burov A. A., Kosenko I. I., Guerman A. D. Dynamics of Moon Elevator. Proceedings of 65th International Astronautical Congress, Toronto, Canada. International Astronautical Federation Paris, France, 2014.

[7] Burov, A.A., Guerman, A.D., Kosenko, I.I. On plane oscillations of a pendulum with variable length suspended on the surface of a planet's satellite. Cosmic Research, Vol. 52(4), 289–294, 2014.

[8] Burov, A.A., Guerman, A.D., Kosenko, I.I. Tether orientation control for lunar elevator. Celestial Mechanics and Dynamical Astronomy, Vol. 120, Issue 3, 337-347, 2014.

[9] Burov, A.A., Guerman, A.D., Kosenko, I.I., Uniform rotations of tethered system connected to a moon surface. Acta Astronautica, Vol. 116, pp. 349-354, 2015.

[10] Burov, A.A., Guerman, A.D., Kosenko, I.I., Ferraz, A., Nikonov, V. Dynamics of space elevator on asteroid. Proceedings of the 66th IAC, Jerusalem, Israel, October 3, IAC-15-D4.3.2,2015.

[11] Puig-Suari, J., Longuski J. M. Tragesser, S. G. "A Tether Sling for Lunar and Interplanetary Exploration." Acta Astronautica, Vol. 36, No 6, pp. 291-295, 1995. (doi:10.1016/0094-5765(95)00110-7).

[12] Thompson, W. B., Stern, M. O. A Skyhook from Phobos to Mars. Proceedings of the 4th International Conference on Tethers in Space, NASA, Washington, DC, pp.1737-1745, 1995.

[13] Penzo, P. A., Mayer, H. L. Tethers and Asteroids for Artificial Gravity assist in the Solar System. Journal of Spacecraft and Rockets. Vol. 23, No 1, pp. 79- 82, 1986. (doi:10.2514/3.25086)

[14] Lanoix, E. L. M. Tether Sling Shot Assists: A Novel Approach to Travelling in the Solar System. Proceedings of the 9th Canadian Aeronautics and Space Institute Conference on Astronautics, Ottawa, Canada, pp.62-71, 1996.

[15] Lanoix, E. L. M., Misra, A. K. Near-Earth Asteroid Missions Using Tether Sling Shot Assist. Journal of Spacecraft and Rockets. Vol. 37, No 4, pp. 475-480, 2000. (doi:10.2514/2.3588).

[16] Prado, A.F.B.A. Using Tethered Gravity Assisted Maneuvers for Planetary Capture, Journal of Guidance, Control and Dynamics. Vol 38, No. 9, pp.1852-1856, 2015. (doi/abs/10.2514/1.G001009).

[17] Prado, A. F. B. A. Tethered Gravity Assisted Maneuvers in Close Approach Asteroids to Accelerate a Spacecraft. AAS paper15-665, 2015.

[18] Prado, A. F. B. A., Gomes, V. M., Chanut, T. G. G. Building an -Escape Portal- with Tethers Fixed in Asteroids. Journal of The Astronautical Sciences, v. 1, p. 1, 2018.

[19] Ferreira, A. F. S., Prado, A. F. B. A., Guerman, A. D., Santos, D. P. S., Burov, A. A., Winter, O C. Using Tethers to Build a "Capture Portal" for the Planet. In: AAS/AIAA Astrodynamics Specialist Conference, 2017, Stevenson, WA. Advances in The Astronautical Sciences. v. 162. p. 3821-3840, 2017.

[20] Ferreira, A. F. S., Prado, A. F. B. A., Guerman, A. D., Santos, D P S, Burov, A. A., Winter, O C. Dynamics of a space tether in binary asteroids. In:

AAS/AIAA Astrodynamics Specialist Conference, 2017, Stevenson, WA. Advances in The Astronautical Sciences, v. 162. p. 3883-3902, 2017.

[21] Scheeres D.J. Orbital motion in strongly perturbed environments: applications to asteroid, comet and planetary satellite orbiters. Berlin: Springer. 2012.

[22] Broucke, R. A. The Celestial Mechanics of Gravity Assist. AIAA Paper 88- 4220, 1988.

[23] Ferreira, A. F. S.; Prado, A. F. B. A. ; Winter, O. C. ; Santos, D. P. S. . Analytical study of the swing-by maneuver in an elliptical system. Astrophysics and Space Science, v. 363, p. 24, 2018.

[24] Prado, A.F.B.A. Powered Swing-By. Journal of Guidance, Control and Dynamics, v. 19, p. 1142-1147, 1996.

[25] Casalino, L, Colasurdo, G., Pastrone, D. Simple Strategy for Powered Swing-By." J. Guid. Control Dynam. Vol. 22, No. 1, 156, 1999.

[26] Ferreira, A. F. S., Kuga, H. K., Prado, A. F. B. A., Winter, O. C. Estimating the trajectory of a space vehicle passing by the Moon using Kalman Filter. Journal of Physics. Conference Series (Print), v. 641, p. 012002, 2015.

[27] Ferreira, A. F. S., Prado, A. F. B. A., Winter, O. C., Santos, D. P. S. Effects of the eccentricity of the primaries in powered Swing-By maneuvers. Advances in Space Research, v. 59, p. 2071-2087, 2017.

[28] Ferreira, A. F. S., Prado, A. F. B. A., Winter, O. C., Santos, D. P. S. Analytical study of the powered Swing-By maneuver for elliptical systems and analysis of its efficiency. Astrophysics and Space Science, v. 363, p. 145, 2018.

[29]Ferreira, A. F. S., Moraes, R. V., Prado, A. F. B. A., Winter, O. C. Trajectory analysis of a spacecraft making a three-dimensional powered swing-by maneuver. In: AAS/AIAA Astrodynamics Specialist Conference, 2018, Snowbird, UT. Advances in The Astronautical Sciences, 2018.

[30] Szebehely, V. Theory of orbits, New York: Academic Press, 1967.

[31] Jet Propulsion Laboratory (JPL). Small-body database browser: 4 Vesta. California: Nasa, 2018. Available in: https://ssd.jpl.nasa.gov/sbdb.cgi#top. Site Manager: Ryan S. Park. Accessed: 14 September 2018.

[32] Jet Propulsion Laboratory (JPL). Small-body database browser: 99942 Apophis. California: Nasa, 2018. Available in: https://ssd.jpl.nasa.gov/sbdb.cgi#top. Site Manager: Ryan S. Park. Accessed: 14 September 2018.